Oxygen abundances in ionized nebulae from photoionization model-fitting

C. Morisset, IA-UNAM

Ionized ISM is an active filter to the ionizing photons

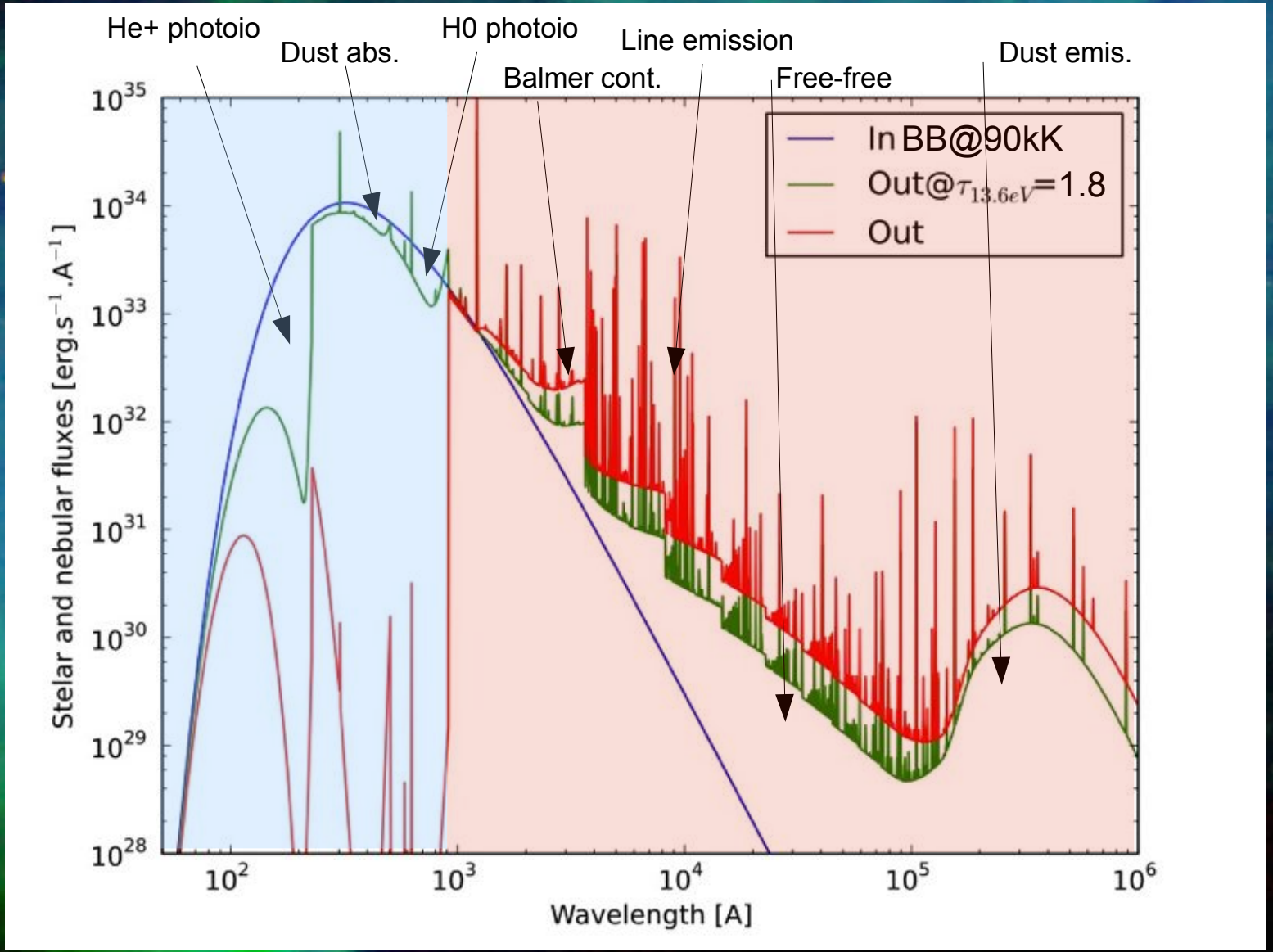

ISM: the two equilibria

- Ionization equilibrium :

  ionization <==> recombination

Photoionization	Radiative recombination
Collisions	Dielectronic recombination
Charge exchange	Charge exchange

- Thermal equilibrium :

  heating <==> cooling

Photoionization	Free-free radiation
Collisions	Free-bound radiation
	Bound-bound radiation

Photoionization codes – first ones

- First models in late 60's by D. Flower, P. Harrington, B. Rubin among others.
- Photoionization codes can be seen as a complete summary of all the physics we know about the interaction between energetic radiation and interstellar gas.

COMPUTER MODELS OF THE PLANETARY NEBULAE NGC 7662 AND IC 418

D. R. FLOWER

Department of Physics, University College, London, England

Discrepancies between the observed and calculated spectra of the nebulae are discussed. There is evidence for the importance of dynamical effects and filamentary structure and possibly for deviations of the flux of the central star of NGC 7662 from black-body values in the far ultra-violet.

Photoionization codes - today

- Today the more used photoionization code is certainly **Cloudy** (G. Ferland, P. van Hoof, R. Porter, R. Williams, W. Henney). It's a 200,000 lines C++ code (with 500,000 lines of data files).
- Some other 1D codes are also used (PHOTO by Stasinska, NEBU by Péquignot, Mapping by Dopita and Binette)
- MOCASSIN (Ercolano) is a Monte-Carlo full 3D code
- Cloudy_3D (IDL and Python versions, by Morisset) is a pseudo-3D code.

Photoionization codes – inputs and outputs

Description of the model (inputs)

- Ionizing SED (BB, stel. model, synth. Spectrum.) T*, L*, Z*
- Gas distribution : nH(r – x,y,z)
- Chemical composition (spatial var?)
- Dust (spatial var?)

Atomic database

- Cross sections
- Recomb. coeffs.
- Collision strengths
- Einstein coeffs.
- Dust properties

PHOTOIONISATION CODE

- Te, ne
- X^i / X (r – x,y,z)
- Line emissivities

Effect of Te on emission lines

For a recombination line, like Hβ:

$$\varepsilon_{H\beta}(T_e) = \frac{4\pi j_{H\beta}}{n_e n_p} = h\nu_{H\beta}\alpha^{eff}_{H\beta}(T_e)$$

For a collisionally-excited line:

$$\varepsilon_{ul}(T_e) = \frac{8.63\times10^{-6}}{T_e^{1/2}}\frac{\gamma_{lu}}{g_u}e^{-h\nu_{ul}/kT}b_{ul}h\nu_{ul}$$

$$\varepsilon_{H\beta} \propto T_e^{-0.9}$$

$$\varepsilon_{ul} \propto T_e^{-0.5}e^{-h\nu_{ul}/kT_e}$$

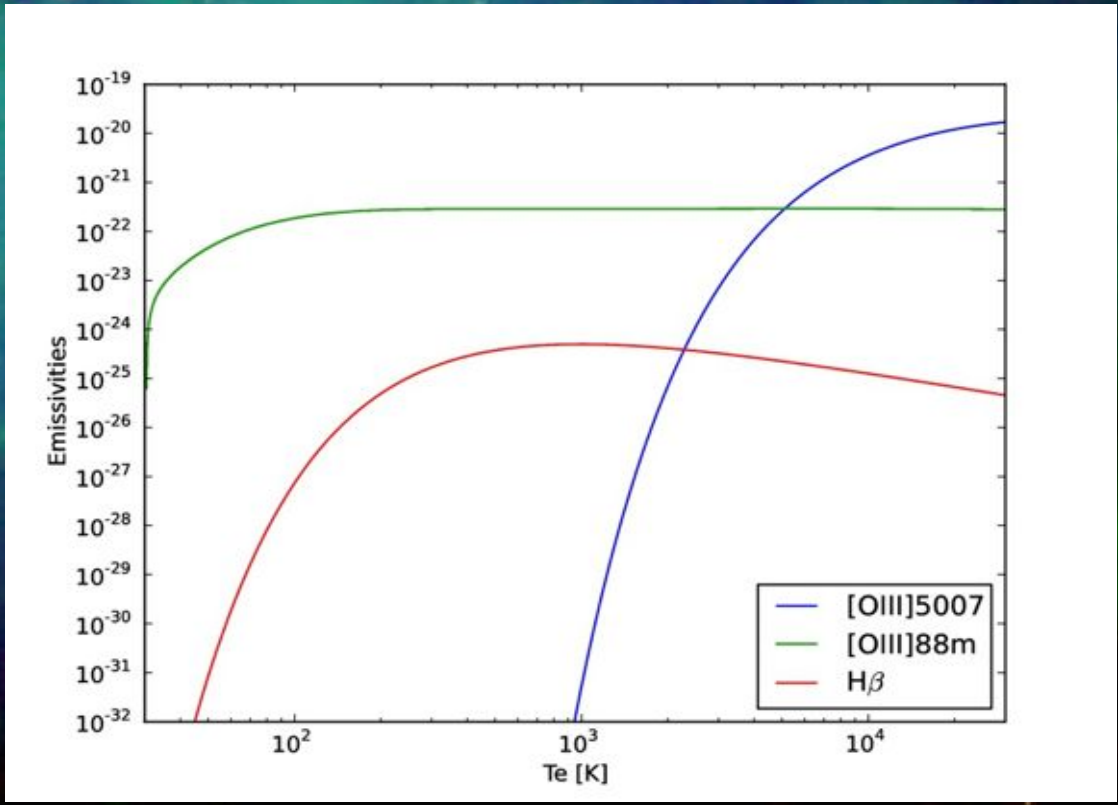

How to make a model ? - basics

Making a model of an given object is finding a (unique?) set of input parameters that are able to reproduce all the observables:

- Emission line ratios (Te- and ne-diagnostics, and also I/Ibeta).
- Absolute value of one emission line intensity.
- Images (shape and angular size – Distance).
- Continuum flux (radio – IR – Opt – UV – X)
- Line profiles, PV-diagrams (velocity field).

How to make a model ? P- and O-spaces

The modeling process can be seen as solving an inverse problem :

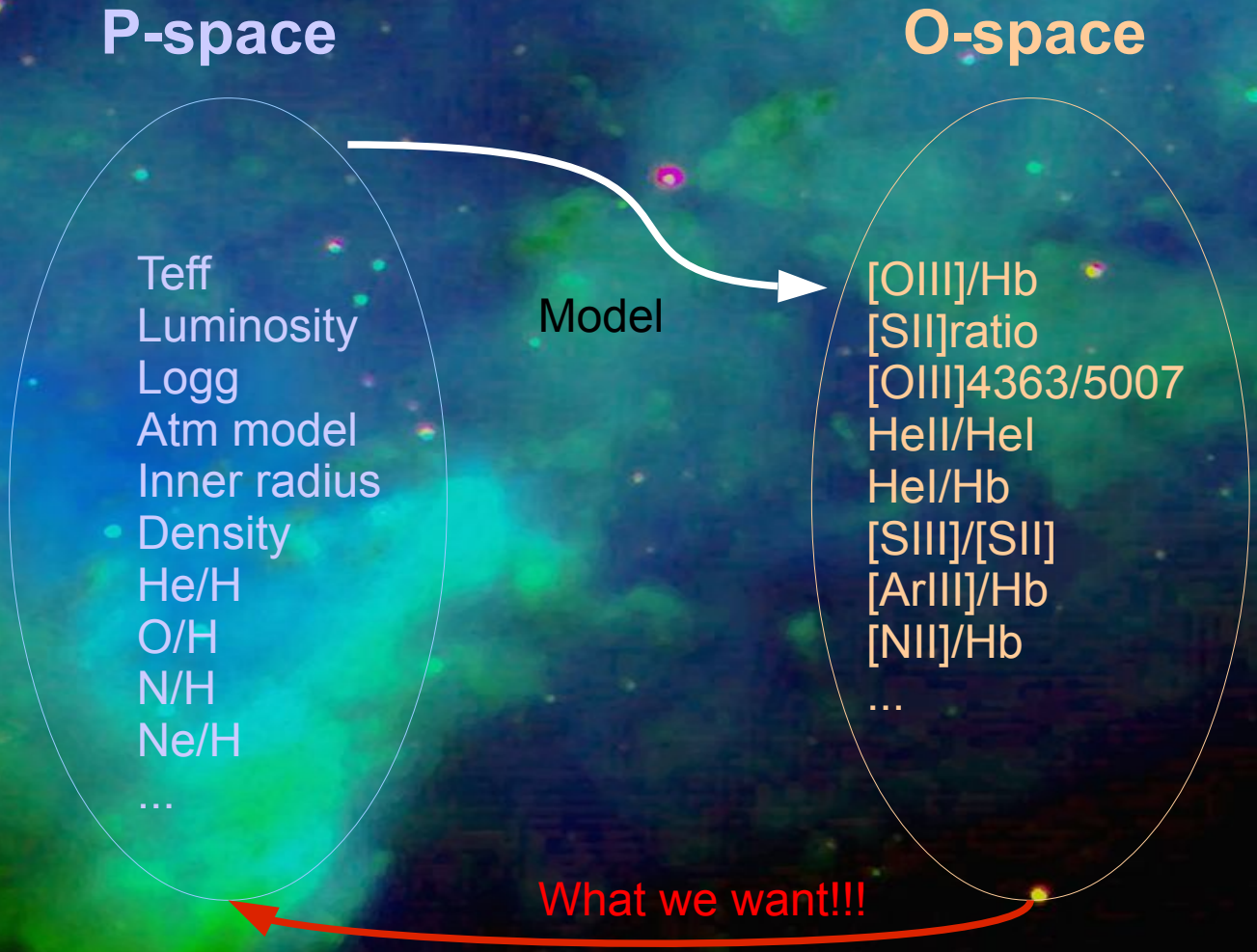

No linearity

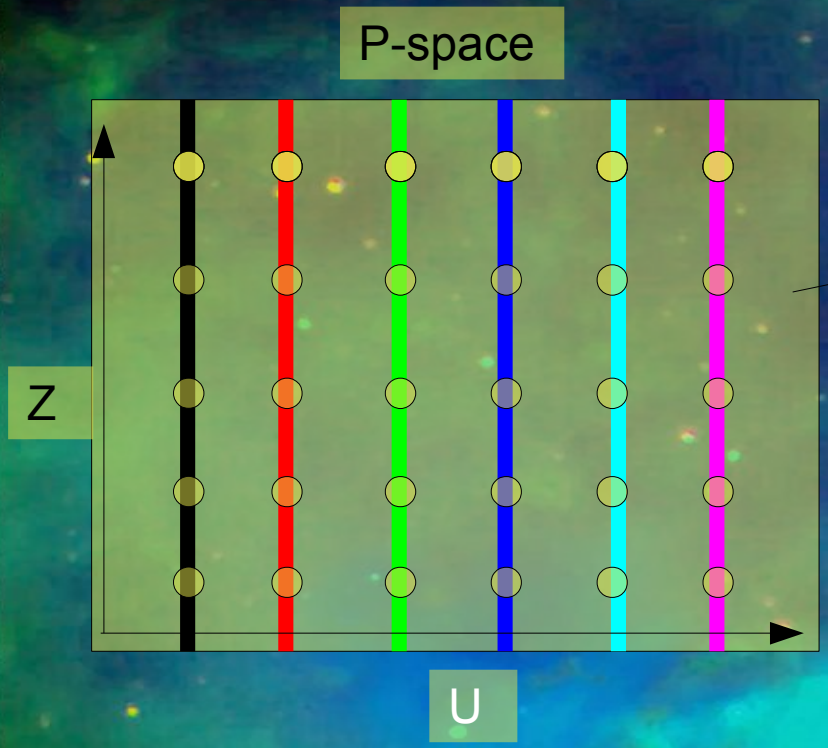

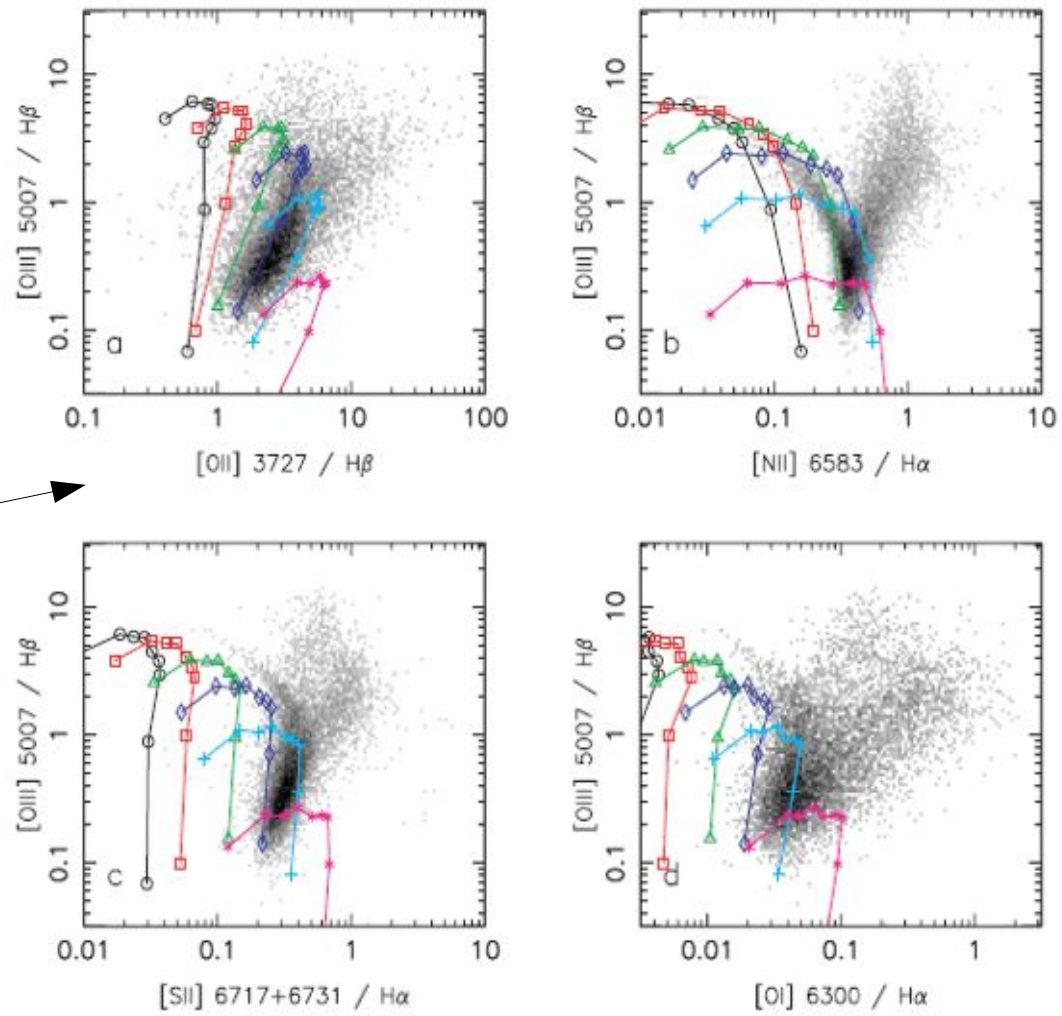

Figure 2. Sequences of photoionization models with varying metallicities Z and constant ionization parameter U. The symbols on the curves correspond to the location of models with metallicities $Z = 0.1$, 0.2, 0.3, 0.4, 0.6, 0.8, 1.0, 1.5 and 2.5 $Z_{\odot}$, going from the upper left to the lower right (in panels b, c and d, the lowest metallicity models are actually outside the range of the plots). The values of the ionization parameter U are 10^{-2} (black circles), 5×10^{-3} (red squares), 2×10^{-3} (green triangles), 10^{-3} (blue diamonds), 5×10^{-4} (cyan + signs) and 2×10^{-4} (purple $*$ signs).

Mon. Not. R. Astron. Soc. 371, 972–982 (2006) doi:10.1111/j.1365-2

Semi-empirical analysis of Sloan Digital Sky Survey galaxies – III. How to distinguish AGN hosts

Grażyna Stasińska,[1*] Roberto Cid Fernandes,[2] Abílio Mateus,[3] Laerte Sodré J. and Natalia V. Asari[2]

How to make a model ?

- The « result » of a model is the set of input parameters, including the density structure, the SED description, the chemical composition, and the temperature and ionic structure.
- There is no ICF, as all the ions are taken into account by the photoionization code, even if not observed.
- Advantage: when a model is converged, abundance can be determine for element from just 1 line!
- It's not easy to define error bars for the resulting parameters. One can run sets of side models to explore the space parameter.

Converging a model: faint lines DO matter

The convergence criterium (manual or automatic) must not only take into account the errors on the lines, but also the importance of the line: [OIII] 5007/4363 must be more important than most of other intense lines / Hbeta.

Converging a model: faint lines DO matter

	A 79		BV 5-1		JnEr 1		M 1-41		NGC 2818		Sh 1-89		Sh 2-71E	
Parameter	Obs.	Model	Obs.	Model	Obs.	Model	Obs.	Model	Obs.	Model	Obs.	Model	Obs.	Model
[O II] λ3727	511	491	352	367	782	734	290	274	509	498	408	385	179	232
[Ne III] λ3869	155	155	163	163	115	112	102	101	155	155	108	112	133	133
Hδ λ4101	30.5	25.8	25.7	25.1	24.5	25.9	25.1	25.4	26.4	25.9	24.5	25.8	23.5	24.7
Hγ λ4340	48.8	46.8	48.3	46.5	57.0	46.9	46.0	46.7	48.0	46.9	45.2	46.8	43.4	46.3
[O III] λ4363	9.19	5.21	25.1	18.2	5.42	4.87	17.2	10.2	14.6	8.06	4.07	3.49	21.4	18.8
He I λ4471	7.19	10.2	6.12	5.99	5.15	7.36	...	4.83	4.40	6.15	4.75	7.16	...	5.96
He II λ4686	48.6	49.8	66.9	68.5	22.9	22.9	53.2	53.0	32.9	32.7	25.7	23.6	90.8	91.3
[Ar IV] λ4740	...	0.35	3.89	3.89	...	0.48	6.92	3.00	...	1.92	...	0.29	8.14	8.54
[O III] λ5007	444	443	951	923	721	820	653	654	808	747	668	691	833	838
[N I] λ5200	34.9	37.0	19.2	19.6	4.84	5.59	22.5	22.6	22.0	23.2	13.3	13.3	24.3	24.8
[Cl III] λ5518	...	1.34	2.59	2.36	...	0.87	...	1.65	...	1.21	...	0.72	...	2.13
[Cl III] λ5538	...	0.99	1.64	1.87	...	0.62	...	1.60	...	0.87	...	0.53	...	1.69
[N II] λ5755	36.1	34.7	26.4	25.0	7.96	6.94	26.1	22.6	19.3	17.3	7.38	8.19	33.8	34.8
He I λ5876	26.9	26.8	16.1	16.1	19.4	19.4	13.7	13.8	16.0	16.1	19.2	19.2	16.1	16.1
[O I] λ6300	98.8	12.5	43.6	10.0	27.3	11.4	43.8	13.7	47.0	16.7	46.3	13.6	25.4	6.58
[S III] λ6312	...	4.86	7.37	9.51	...	0.52	7.75	5.22	2.83	4.46	...	1.43	9.64	15.4
Hα λ6563	291	291	299	299	290	290	296	296	289	289	292	292	302	302
[N II] λ6584	2155	2050	1135	1101	633	584	1010	1011	1175	1191	793	813	1614	1615
He I λ6678	10.4	7.51	4.73	4.35	...	5.49	3.58	3.54	4.86	4.55	5.56	5.42	6.83	4.35
[S II] λ6717	145	144	99.0	98.1	16.4	16.8	48.7	48.7	114	115	47.7	48.5	106	107
[S II] λ6731	117	116	94.9	94.2	11.4	11.8	66.1	66.2	82.5	83.3	40.2	40.8	101	102
[Ar V] λ7006	...	...	2.10	0.36	...	...	5.80	0.17	...	0.51	...	...	...	1.82
[Ar III] λ7136	33.5	33.2	44.6	44.6	28.0	27.2	62.1	62.2	31.6	31.4	15.1	15.3	59.1	59.1
C(Hβ)	0.37	...	0.80	...	0.21	...	1.99	...	0.20	...	1.00	...	0.67	...
T(N II)	10937	10983	12702	12535	10996	10726	12997	12070	10884	10326	8625	8915	12046	12229
T(O III)	15529	12272	17528	15183	10524	9791	17461	13638	14599	11891	9862	9338	17284	16117
N_e	194	195	549	552	20	20	2059	2010	31	36	251	250	524	535
rms	...	0.10	...	0.07	...	0.08	...	0.12	...	0.13	...	0.08	...	0.12
log [L(Hα)]	...	34.8	...	35.1	...	33.8	...	34.9	...	34.6	...	34.6	...	35.1
D(L)	...	6.5	...	7.1	...	0.9	...	1.3	...	3.2	...	1.9	...	5.4
D(R)	...	1.8	...	2.7	...	1.3	...	0.4	...	4.9	...	0.8	...	1.0
[C I] λ9850	...	6.95	...	1.08	...	14.6	...	11.3	...	4.65	...	87.8	...	1.81
[C II] λ2326	...	56.6	...	30.3	...	71.7	...	281	...	30.7	...	447	...	41.1
[C III] λ1909	...	106	...	166	...	119	...	1066	...	96.2	...	711	...	406
[C IV] λ1549	...	4.20	...	45.1	...	8.97	...	133	...	45.1	...	31.4	...	252
[N III] λ1750	...	72.2	...	264	...	7.53	...	120	...	9.68	...	9.68	...	707
[N III] 57.21 μm	...	295	...	207	...	216	...	67.4	...	361	...	275	...	405
[N IV] λ1486	...	3.80	...	70.7	...	1.00	...	20.3	...	41.4	...	0.93	...	488
[O IV] 25.88 μm	...	15.9	...	109	...	67.6	...	48.1	...	152	...	66.0	...	177
[Ne IV] λ2424	...	2.84	...	30.2	...	1.20	...	8.92	...	22.4	...	1.44	...	61.3
[Ne V] 14.32 μm	...	0.17	...	7.59	...	...	...	1.82	...	12.2	...	0.41	...	20.7
[S III] λ9532	...	131	...	175	...	21.7	...	111	...	134	...	67.5	...	262
[S IV] 10.51 μm	...	12.1	...	63.4	...	5.06	...	28.3	...	58.9	...	19.6	...	150
[Cl IV] λ8047	...	1.27	...	2.17	...	1.29	...	1.81	...	1.15	...	0.75	...	1.94

Converging a model: faint lines DO matter

Parameter	A 79		BV 5-1		JnEr 1		M 1-41		NGC 2818		Sh 1-89		Sh 2-71E	
	Obs.	Model	Obs.	Model	Obs.	Model	Obs.	Model	Obs.	Model	Obs.	Model	Obs.	Model
[O II] λ3727	511	491	352	367	782	734	290	274	509	498	408	385	179	232
[Ne III] λ3869	155	155	163	163	115	112	102	101	155	155	108	112	133	133
Hδ λ4101	30.5	25.8	25.7	25.1	24.5	25.9	25.1	25.4	26.4	25.9	24.5	25.8	23.5	24.7
Hγ λ4340	48.8	46.8	48.3	46.5	57.0	46.9	46.0	46.7	48.0	46.9	45.2	46.8	43.4	46.3
[O III] λ4363	9.19	5.21	25.1	18.2	5.42	4.87	17.2	10.2	14.6	8.06	4.07	3.49	21.4	18.8
He I λ4471	7.19	10.2	6.12	5.99	5.15	7.36	...	4.83	4.40	6.15	4.75	7.16	...	5.96
He II λ4686	48.6	49.8	66.9	68.5	22.9	22.9	53.2	53.0	32.9	32.7	25.7	23.6	90.8	91.3
[Ar IV] λ4740	...	0.35	3.89	3.89	...	0.48	6.92	3.00	...	1.92	...	0.29	8.14	8.54
[O III] λ5007	444	443	951	923	721	820	653	654	808	747	668	691	833	838
[N I] λ5200	34.9	37.0	19.2	19.6	4.84	5.59	22.5	22.6	22.0	23.2	13.3	13.3	24.3	24.8
[Cl III] λ5518	...	1.34	2.59	2.36	...	0.87	...	1.65	...	1.21	...	0.72	...	2.13
[Cl III] λ5538	...	0.99	1.64	1.87	...	0.62	...	1.60	...	0.87	...	0.53	...	1.69
[N II] λ5755	36.1	34.7	26.4	25.0	7.96	6.94	26.1	22.6	19.3	17.3	7.38	8.19	33.8	34.8
He I λ5876	26.9	26.8	16.1	16.1	19.4	19.4	13.7	13.8	16.0	16.1	19.2	19.2	16.1	16.1
[O I] λ6300	98.8	12.5	43.6	10.0	27.3	11.4	43.8	13.7	47.0	16.7	46.3	13.6	25.4	6.58
[S III] λ6312	...	4.86	7.37	9.51	...	0.52	7.75	5.22	2.83	4.46	...	1.43	9.64	15.4
Hα λ6563	291	291	299	299	290	290	296	296	289	289	292	292	302	302
[N II] λ6584	2155	2050	1135	1101	633	584	1010	1011	1175	1191	793	813	1614	1615
He I λ6678	10.4	7.51	4.73	4.35	...	5.49	3.58	3.54	4.86	4.55	5.56	5.42	6.83	4.35
[S II] λ6717	145	144	99.0	98.1	16.4	16.8	48.7	48.7	114	115	47.7	48.5	106	107
[S II] λ6731	117	116	94.9	94.2	11.4	11.8	66.1	66.2	82.5	83.3	40.2	40.8	101	102
[Ar V] λ7006	...	...	2.10	0.36	...	...	5.80	0.17	...	0.51	...	...	...	1.82
[Ar III] λ7136	33.5	33.2	44.6	44.6	28.0	27.2	62.1	62.2	31.6	31.4	15.1	15.3	59.1	59.1
$C(H\beta)$	0.37	...	0.80	...	0.21	...	1.99	...	0.20	...	1.00	...	0.67	...
$T(N II)$	10937	10983	12702	12535	10996	10726	12997	12070	10884	10326	8625	8915	12046	12229
$T(O III)$	15529	12272	17528	15183	10524	9791	17461	13638	14599	11891	9862	9338	17284	16117
N_e	194	195	549	552	20	20	2059	2010	31	36	251	250	524	535
rms	...	0.10	...	0.07	...	0.08	...	0.12	...	0.13	...	0.08	...	0.12
log [$L(H\alpha)$]	...	34.8	...	35.1	...	33.8	...	34.9	...	34.6	..			
$D(L)$	...	6.5	...	7.1	...	0.9	...	1.3	...	3.2	..			
$D(R)$	...	1.8	...	2.7	...	1.3	...	0.4	...	4.9	..			
[C I] λ9850	...	6.95	...	1.08	...	14.6	...	11.3	...	4.65	..			
[C II] λ2326	...	56.6	...	30.3	...	71.7	...	281	...	30.7	..			
[C III] λ1909	...	106	...	166	...	119	...	1066	...	96.2	..			
[C IV] λ1549	...	4.20	...	45.1	...	8.97	...	133	...	45.1	..			
[N III] λ1750	...	72.2	...	264	...	7.53	...	120	...	9.68	..			
[N III] 57.21 μm	...	295	...	207	...	216	...	67.4	...	361	..			
[N IV] λ1486	...	3.80	...	70.7	...	1.00	...	20.3	...	41.4	..			
[O IV] 25.88 μm	...	15.9	...	109	...	67.6	...	48.1	...	152	..			
[Ne IV] λ2424	...	2.84	...	30.2	...	1.20	...	8.92	...	22.4	..			
[Ne V] 14.32 μm	...	0.17	...	7.59	...	...	...	1.82	...	12.2	..			
[S III] λ9532	...	131	...	175	...	21.7	...	111	...	134	..			
[S IV] 10.51 μm	...	12.1	...	63.4	...	5.06	...	28.3	...	58.9	..			
[Cl IV] λ8047	...	1.27	...	2.17	...	1.29	...	1.81	...	1.15	..			

The rms relative difference between the observed and modeled spectra was determined with

$$\mathrm{rms}^2 = \frac{1}{N}\sum W_i \frac{(O_i - M_i)^2}{O_i^2}, \qquad (2)$$

where N is the number of lines included in the analysis, W_i is a line weight factor, and O_i and M_i are the observed and modeled line intensities. The line weight factor is equal to 1 when $O_i/H\beta > 0.5$, 0.5 if $O_i/H\beta \in [0.1, 0.5)$ and 0.25 if $O_i/H\beta \in [0.01, 0.1)$. Obviously, all hydrogen recombination lines are ex-

Comparing with direct method

- Direct method :
  - Determine Te, ne (line ratios)
  - Determine ionic abundances
  - Determine element abundances (ICF from... photoionization model, e.g KB94!)
- Photoionization model :
  - Set nH(R), abundances, SED, Dust
  - Fits observables

quite heavy !

Comparing with direct method

If the nebula is iso-Te and iso-ne, one should obtain the same ionic abundances with both methods (the same physics apply).

Advantages of photoionization models

- Aperture effects
- SED effects
- Multi components model
- Dust effect
- Te natural gradient
- ICF included
- Multiple stars

Aperture effects

A photoionization model of the compact H II region G29.96-0.02*

C. Morisset[1], D. Schaerer[2], N. L. Martín-Hernández[3], E. Peeters[3,4], F. Damour[1], J.-P. Baluteau[1], P. Cox[5], and P. Roelfsema[4]

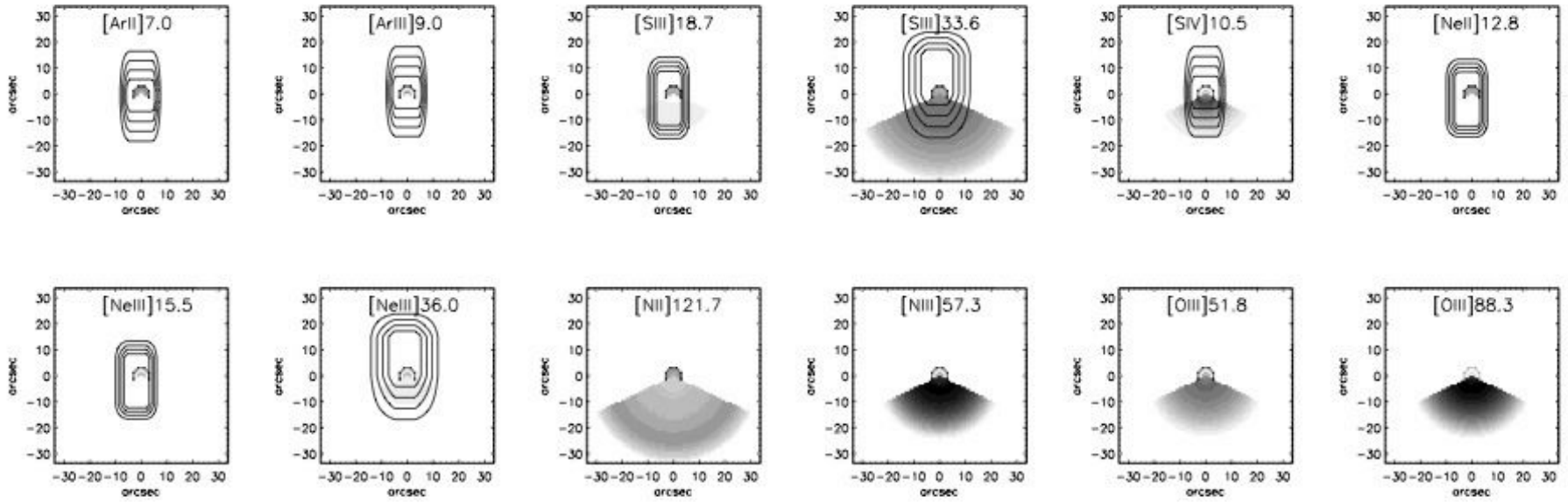

Fig. 1. Emission lines maps of the best model, in grey linear scale. The two components are presented with angular size related to their corresponding covering factors. Contours for the ISO *SWS* beam profile are superposed, for transmissions of 20, 40, 60, 80% of the flux. In the four latest maps, the *LWS* aperture size is of order of the images, and not shown. Note that the *SWS* aperture is not always centered.

In the case of slits smaller than the object, it very important to determine the angular distribution of the emission for each line.

Aperture effects

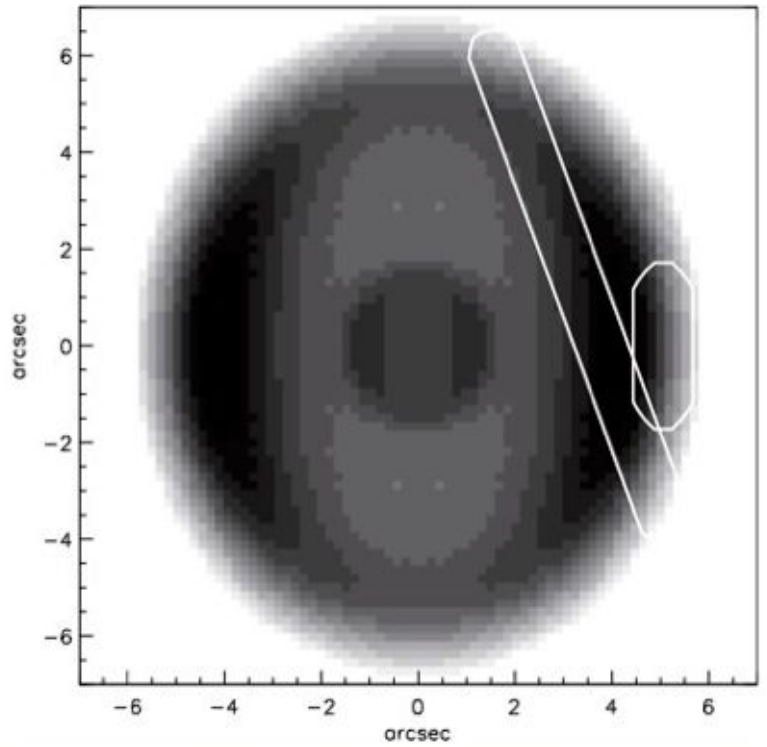

Fig. 3. Apertures used to reproduce observations by Sharpee et al. (2004) (left one) and Hyung et al. (1994) (right one), superimposed on the Hβ model image.

A self-consistent stellar and 3D nebular model of planetary nebula IC 418*

C. Morisset and L. Georgiev

He I 7065	0	**7.040**	8.266	[O II] 7332	3	**13.380**	14.613
He I 7065	4	**5.130**	7.867	O I 7773	0	**0.075**	0.054
He I 7281	0	**0.791**	0.683	O I 8447[a]	0	**1.142**	0.007
[C I] 8727	0	**0.033**	0.030	O I 9264	0	**0.027**	0.020
[C II] 157.	1	**1.100**	0.403	[O III] 4363	0	**0.935**	0.710
C II] 2326	2	**81.462**	88.482	[O III] 4363	3	**0.520**	0.421
C III] 1909	2	**27.592**	34.878	[O III] 4363	4	**0.910**	0.716
C II 1335	2	**23.212**	20.164	[O III] 4959	0	**72.700**	65.158
C II 1761[a]	2	**2.102**	0.349	[O III] 4959	3	**29.520**	37.300
C II 4267	0	**0.570**	0.452	[O III] 4959	4	**50.100**	65.034
C II 4267	4	**0.690**	0.436	[O III] 5007	0	**214.000**	196.126
C II 4619	0	**0.011**	0.021	[O III] 5007	3	**85.870**	112.273
C II 6580[a]	0	**0.805**	0.039	[O III] 5007	4	**151.000**	195.754
C II 7231[a]	0	**0.169**	0.006	[O III] 51.8	1	**15.261**	13.430
[N I] 5198	0	**0.201**	0.046	[O III] 88.3	1	**2.407**	1.854
[N I] 5200	0	**0.117**	0.016	O II 4152	0	**0.018**	0.023
[N II] 5755	0	**2.760**	2.599	O II 4341	0	**0.085**	0.091
[N II] 5755	3	**3.910**	3.723	O II 4593[a]	0	**0.024**	0.004
[N II] 5755	4	**2.190**	2.694	O II 4651	0	**0.171**	0.172
[N II] 6548	0	**53.600**	53.094	[Ne II] 12.8	1	**53.098**	61.004
[N II] 6548	3	**71.230**	73.639	[Ne III] 3869	0	**3.090**	2.806
[N II] 6548	4	**51.300**	54.902	[Ne III] 3869	3	**2.050**	1.147
[N II] 6584	0	**162.900**	156.681	[Ne III] 3869	4	**2.630**	3.766
[N II] 6584	3	**206.830**	217.309	[Ne III] 3968	0	**0.970**	0.846
[N II] 6584	4	**151.000**	162.014	[Ne III] 3968	3	**0.640**	0.346
[N II] 121.	1	**0.283**	0.189	[Ne III] 15.5	1	**9.512**	9.276

Discrepancies between different observations not always mean errors... Can be due to the slit size and position.

SED effect

Mid-IR observations of Galactic H II regions: Constraining ionizing spectra of massive stars and the nature of the observed excitation sequences

C. Morisset[1,2], D. Schaerer[3,4], J.-C. Bouret[2], and F. Martins[4,3]

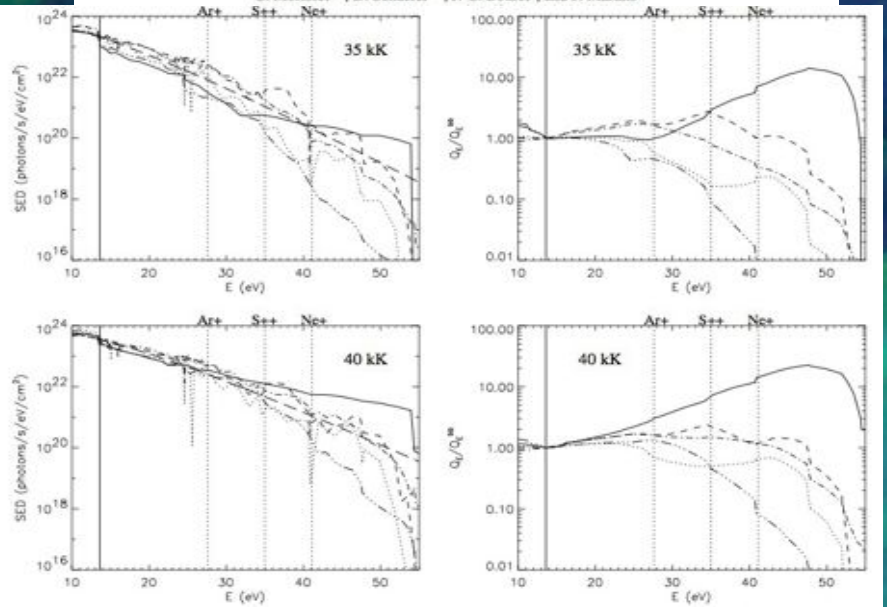

Fig. 2. Comparison between the 6 stellar atmosphere models: *CoStar* (solid), *WM-Basic* (dotted), *CMFGEN* (dashed), *TLUSTY* (dash dot), *Kurucz* (dash dot dot) and the Blackbody (long dashes, left panels only), for the same $T_{\rm eff}$ of 35 kK (upper plots), except for *CoStar* model (see text), and 40 kK (lower plots). The left panels show the Spectral Energy Distribution and the right panels show, for any energy E (eV), the number Q_E of photons with energy greater than E, relative to the corresponding number for the Blackbody emission, all the spectra having the same value for $Q_{13.6}$. Vertical lines are plotted at 13.6 eV (solid) and 27.6, 35.0 and 41.1 eV (dotted), corresponding to the ionization potentials of the ions considered in this paper (Ar^+, S^{++}, and Ne^+ resp.).

The ionizing radiation from massive stars and its impact on HII regions: results from modern model atmospheres

S. Simón-Díaz[1,2] ⋆ and G. Stasińska[1]

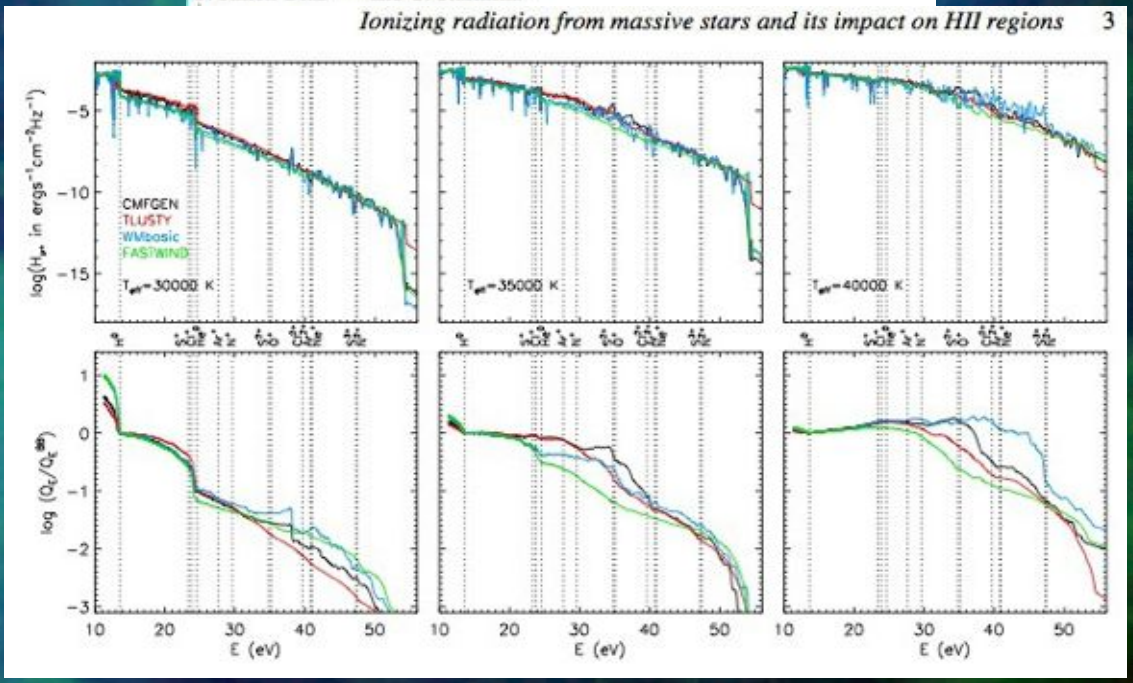

Atmosphere models almost always agree in the optical and near UV (observed part of the SED), but can strongly disagree in the never-observed ionizing part of the SED. The nebula « see » this, and tell us about the SED shape.

2-components models

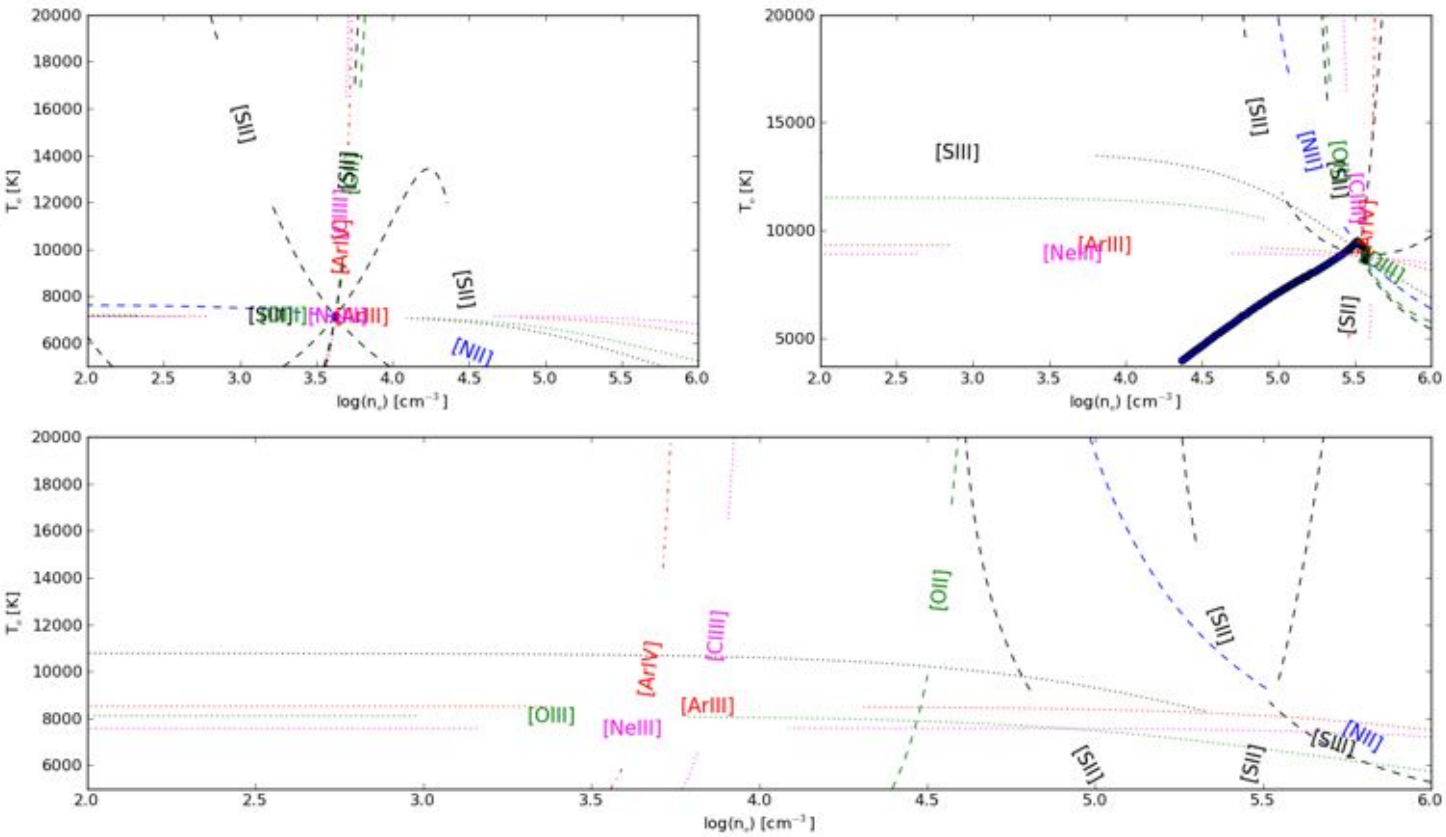

- 2 components, differing by Te, ne and the ionization structure.
- No way to separate them without a detail model.

Metal-rich inclusions

Three-dimensional chemically homogeneous and bi-abundance photoionization models of the 'super-metal-rich' planetary nebula NGC 6153

H.-B. Yuan,[1] X.-W. Liu,[1,2★] D. Péquignot,[3] R. H. Rubin,[2,4,5] B. Ercolano[6,7,8] and Y. Zhang[9]

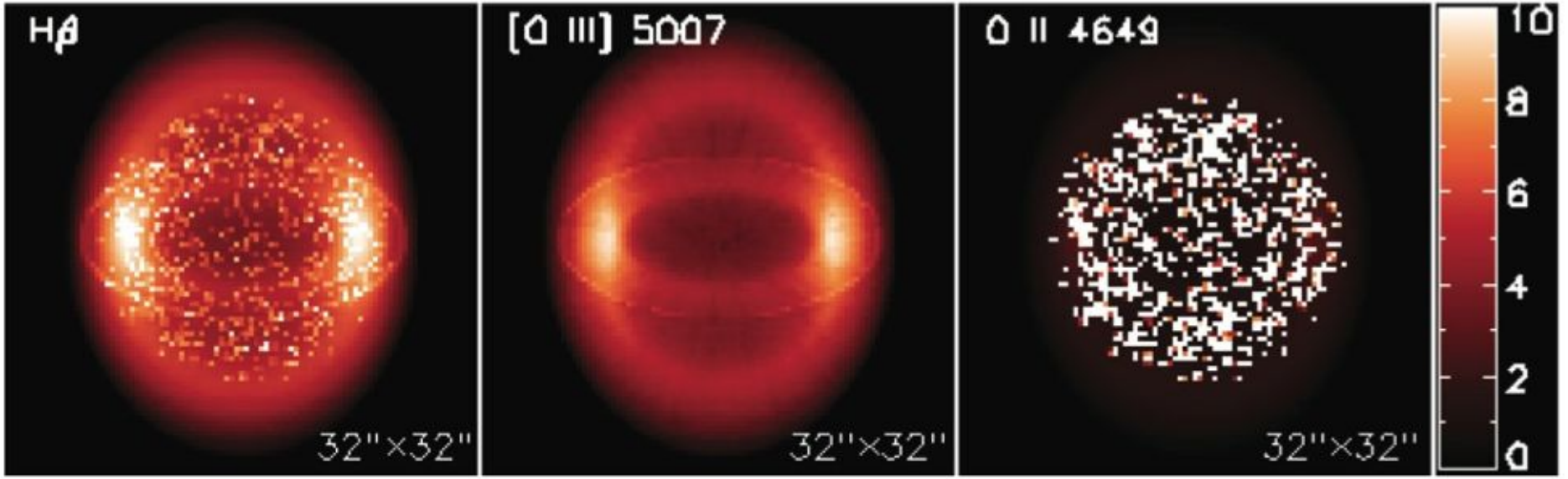

Figure 14. Projected monochromatic images of Hβ (left-hand panel), [O III] λ5007 (central panel) and O II λ4649 (right-hand panel) predicted by the bi-abundance model B at a viewing angle of $\theta = 60°$. $\theta = 0°$ is for face on. The units of the colour bars are 10^{-13}, 10^{-12} and 10^{-15} erg cm^{-2} s^{-1} arcsec^{-2} for the three images, respectively.

Metal-rich inclusions

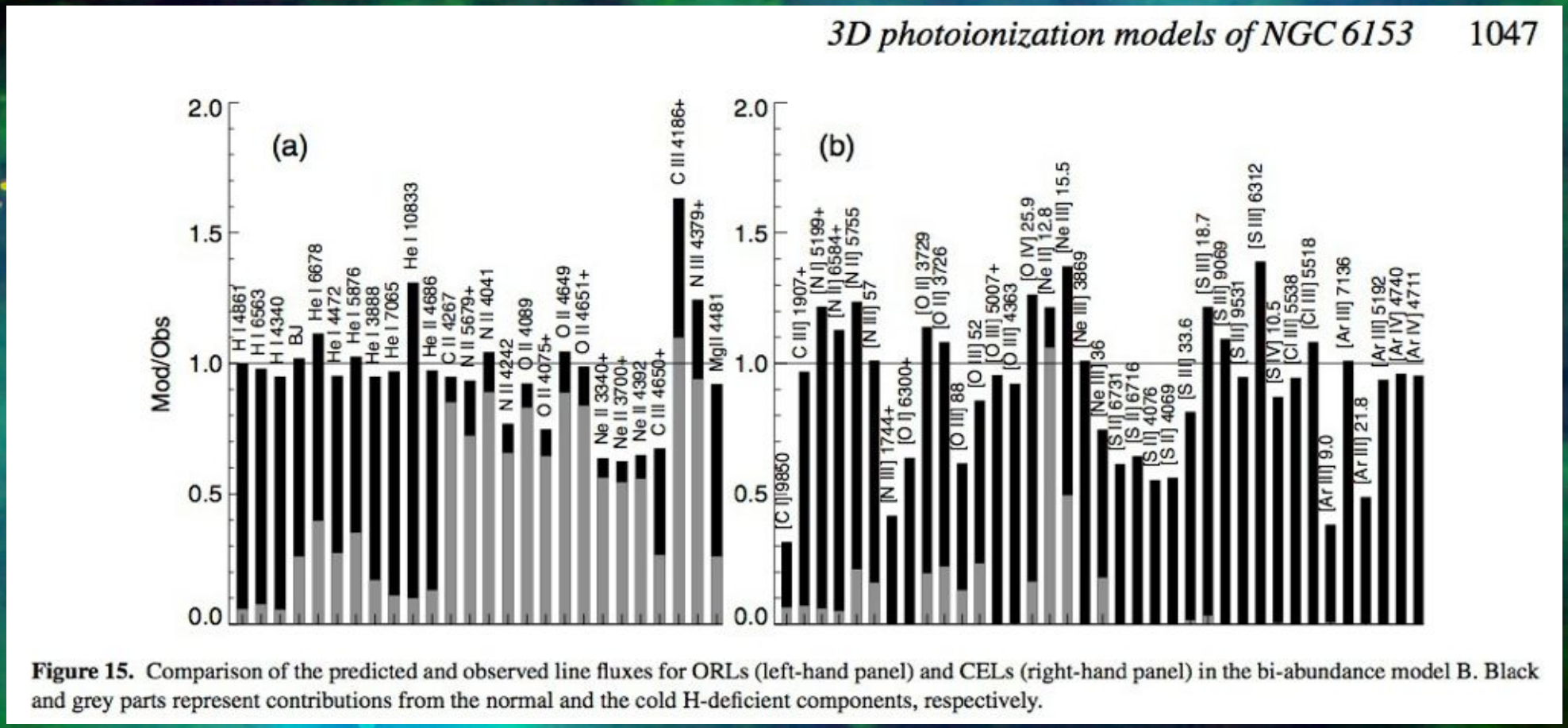

Figure 15. Comparison of the predicted and observed line fluxes for ORLs (left-hand panel) and CELs (right-hand panel) in the bi-abundance model B. Black and grey parts represent contributions from the normal and the cold H-deficient components, respectively.

A kind of 2-components model. Direct method is not usable, unless one have a way to separate the contribution of each component in each emission line.

Effect of the dust

Table 5. Abundances determination for models with $T_* = 5 \times 10^4$ K.

	model Aa	model Ba	model Ca	model Da	model Ea	model Fa	model Ga
$T_{r[O\,III]}$	8242.	8552.	13 504.	9356.	8330.	8422.	13 145.
$T_{r[N\,II]}$	8197.	8434.	10 480.	9079.	8776.	9051.	11 334.
$n_{e[S\,II]}$	9120.	8837.	6832.	7444.	6548.	14 782.	10 108.
$n_{e[Ar\,IV]}$	11 120.	11 091.	10 949.	11 012.	20 401.	13 830.	12 338.
$He^+(\lambda5876)/H^+$	1.11E-01	1.13E-01	1.07E-01	1.14E-01	1.12E-01	1.12E-01	1.08E-01
$He^{++}(\lambda4686)/H^+$	1.34E-04	1.88E-04	7.36E-04	2.03E-04	1.37E-04	1.35E-04	6.18E-04
He/H	1.12E-01	1.14E-01	1.08E-01	1.15E-01	1.12E-01	1.12E-01	1.08E-01
$O^+(\lambda3727)/H^+$	1.20E-04	1.12E-04	7.04E-05	8.23E-05	6.34E-05	8.83E-05	5.55E-05
$O^{++}(\lambda5007)/H^+$	3.26E-04	3.30E-04	2.61E-04	3.32E-04	3.57E-04	2.77E-04	2.18E-04
$O^{++}(\lambda1663)/H^+$	3.37E-04	3.42E-04	3.08E-04	3.56E-04	3.71E-04	2.73E-04	2.63E-04
$O^{++}(\lambda52\,\mu m)/H^+$	3.27E-04	3.31E-04	3.08E-04	3.43E-04	4.04E-04	2.66E-04	2.25E-04
$O^{++}(\lambda88\,\mu m)/H^+$	3.26E-04	3.30E-04	3.05E-04	3.42E-04	4.17E-04	2.83E-04	2.35E-04
$O^{++}(\lambda4651)/H^+$	3.28E-04	3.33E-04	3.48E-04	3.53E-04	3.56E-04	2.92E-04	3.06E-04
O/H	4.47E-04	4.43E-04	3.32E-04	4.15E-04	4.21E-04	3.66E-04	2.75E-04
C/O	1.29E+00	1.28E+00	1.17E+00	1.23E+00	1.28E+00	1.31E+00	1.19E+00
N/O	4.14E-01	4.20E-01	5.21E-01	4.70E-01	5.23E-01	5.67E-01	6.86E-01
Ne/O	2.62E-01	2.65E-01	2.73E-01	2.68E-01	2.59E-01	2.71E-01	2.83E-01

Dust changes the temperature structure of the nebulae. In this study, Stasinska & Szczerba test different dust (small, large grains, inclusions) and found that the derived O/H abundance is strongly affected (input value = 4.79E-04). AND DEPLETION EFFECT...

Temperature gradient

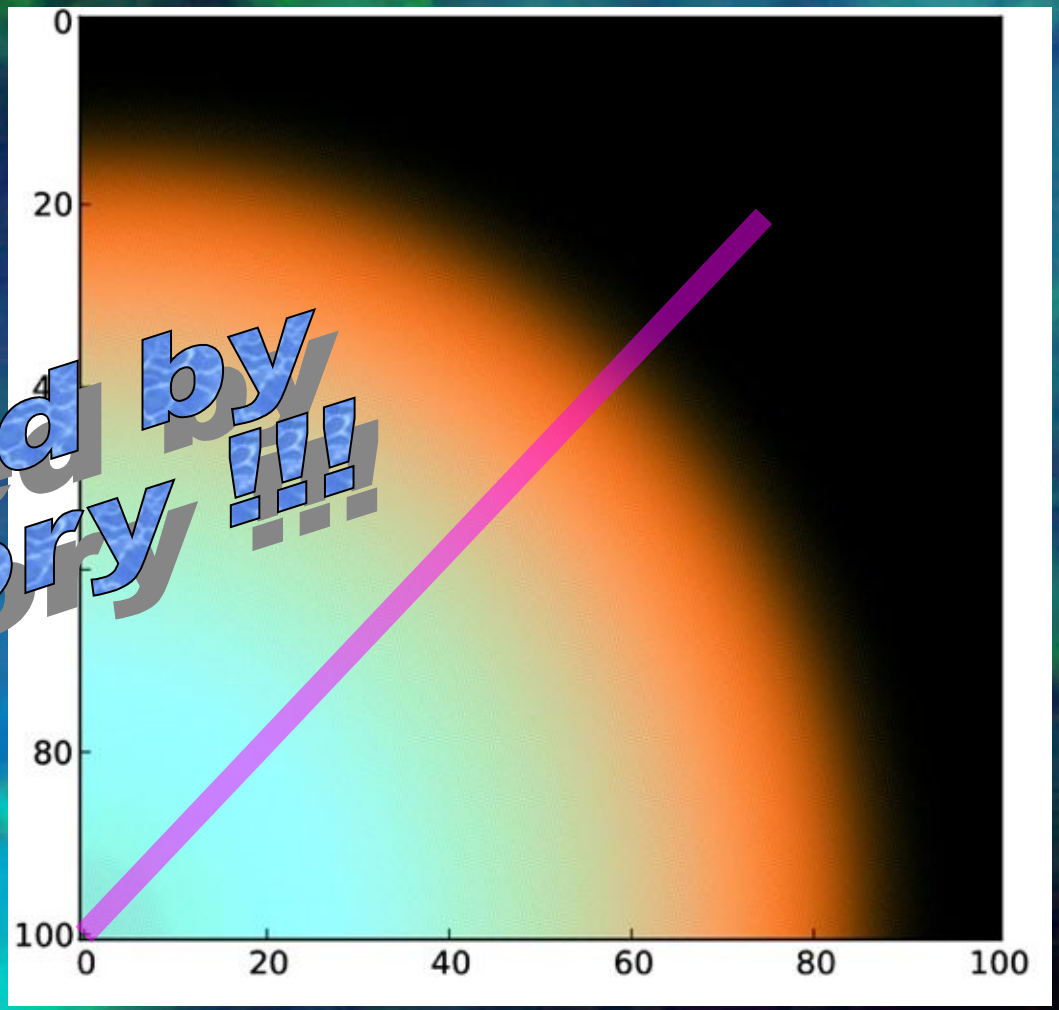

Inspired by true story !!!

R([OII]), G(HI) B([OIII]) image of the 3D model

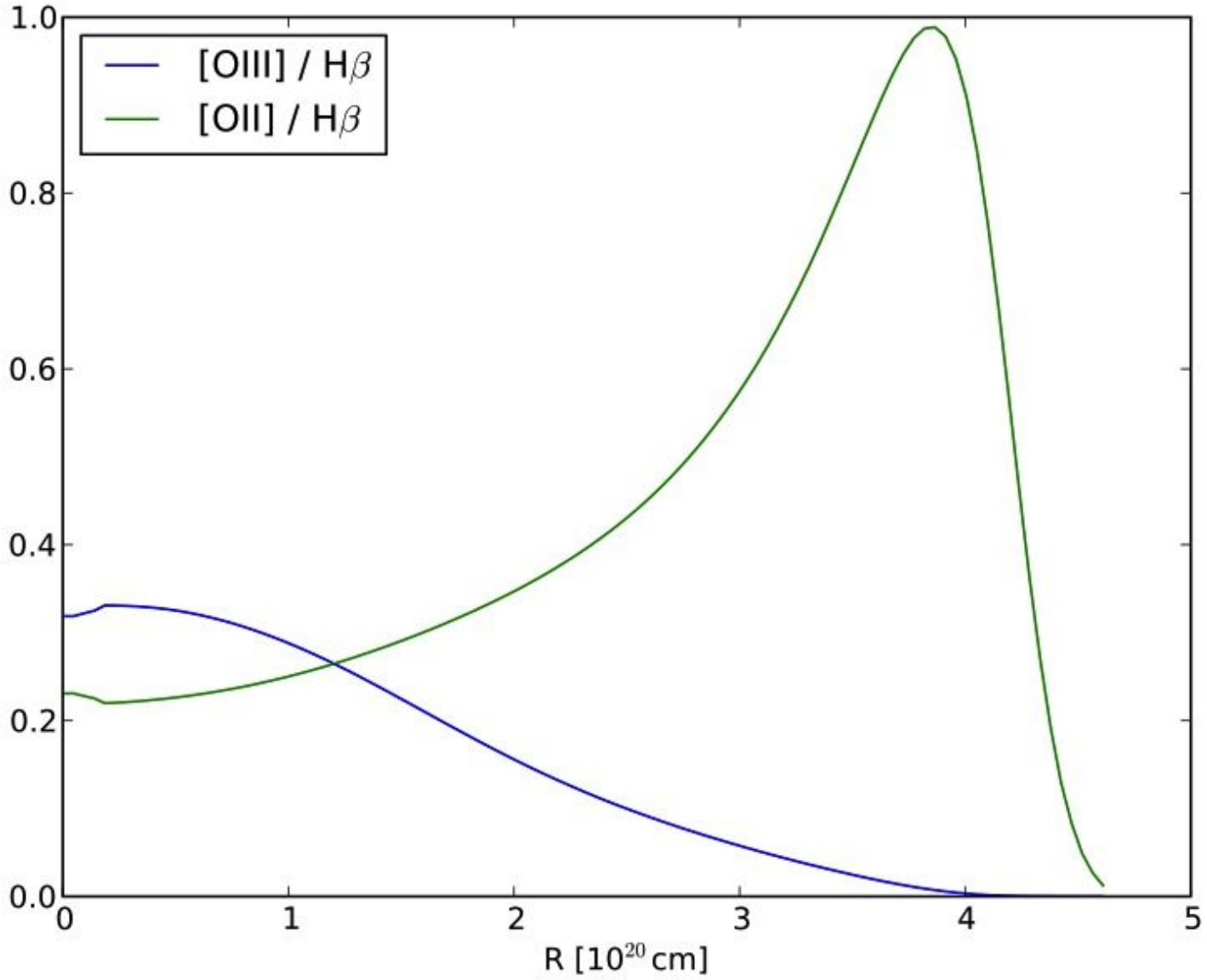

Emission line radial profile, obtained through a « virtual » slit on the model monochromatic images.

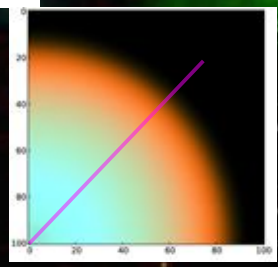

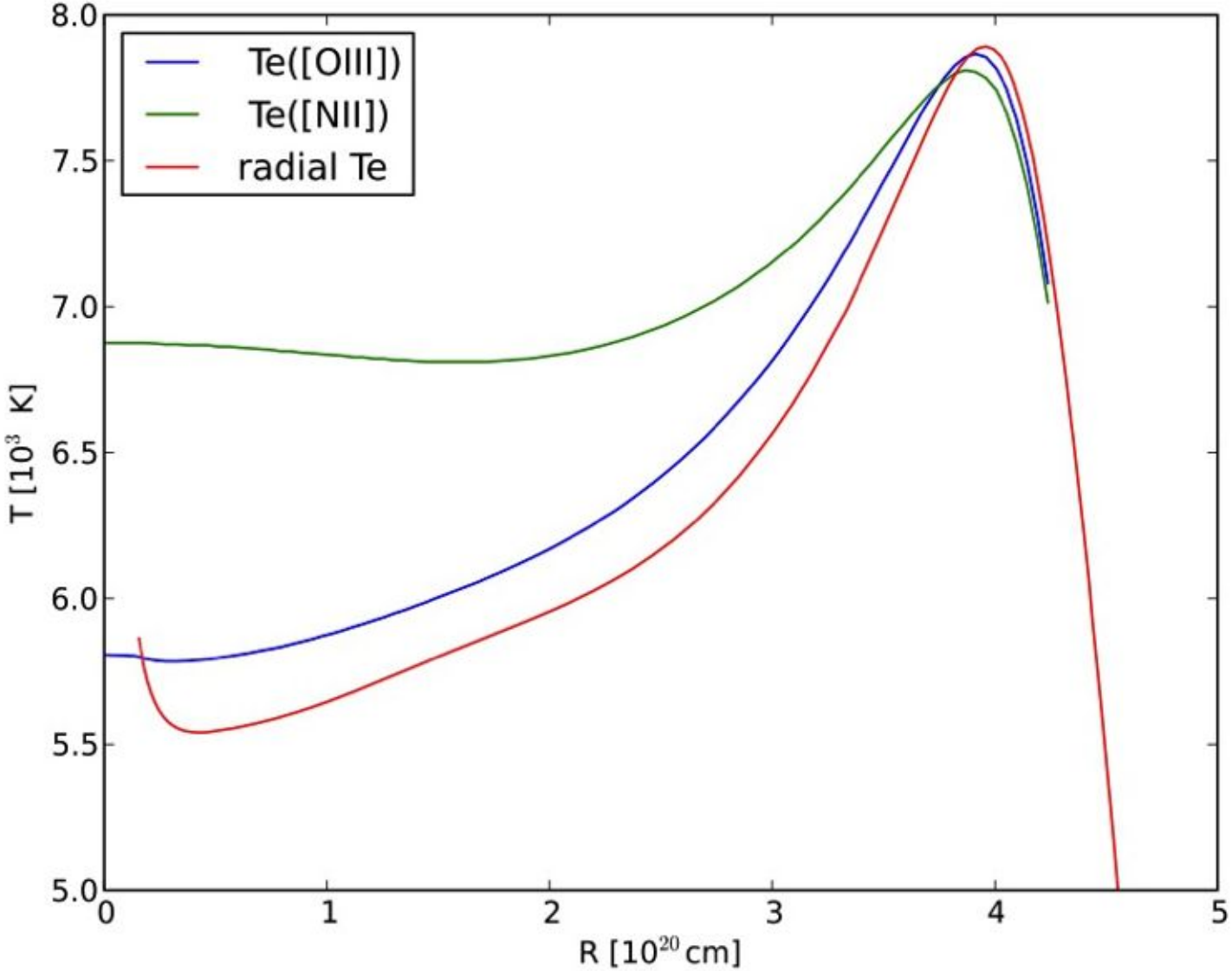

Radial profile of the electron temperature, obtained through a « virtual » slit on the model monochromatic images.

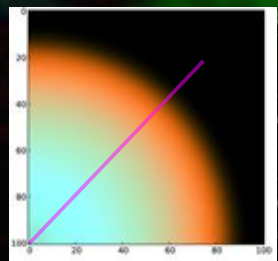

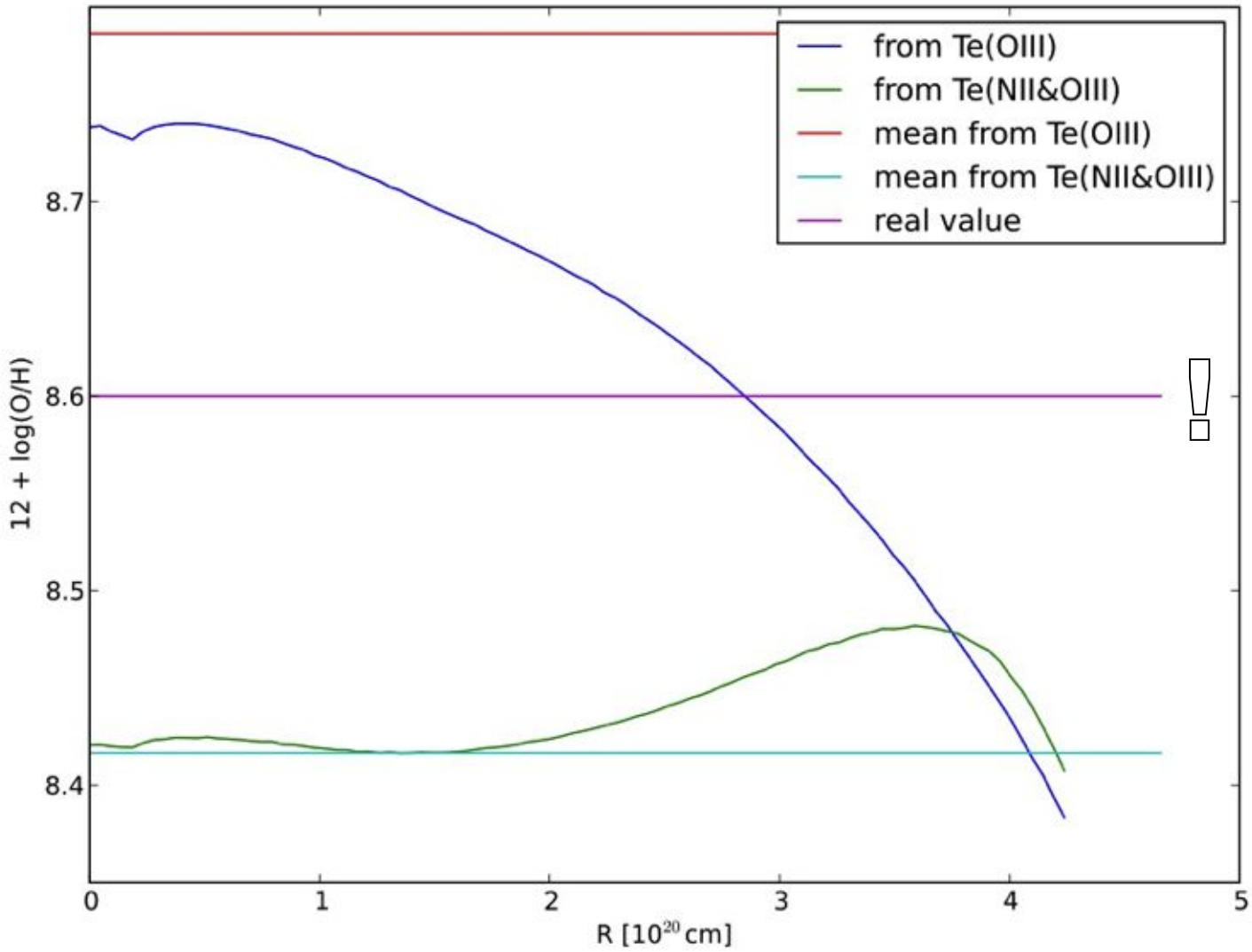

Radial profile of the Oxygen abundance, obtained through a « virtual » slit on the model monochromatic images.

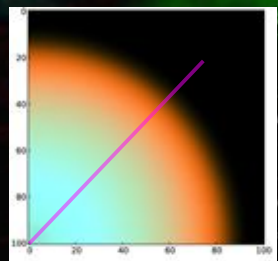

Normal N/H abundance in FLIERS

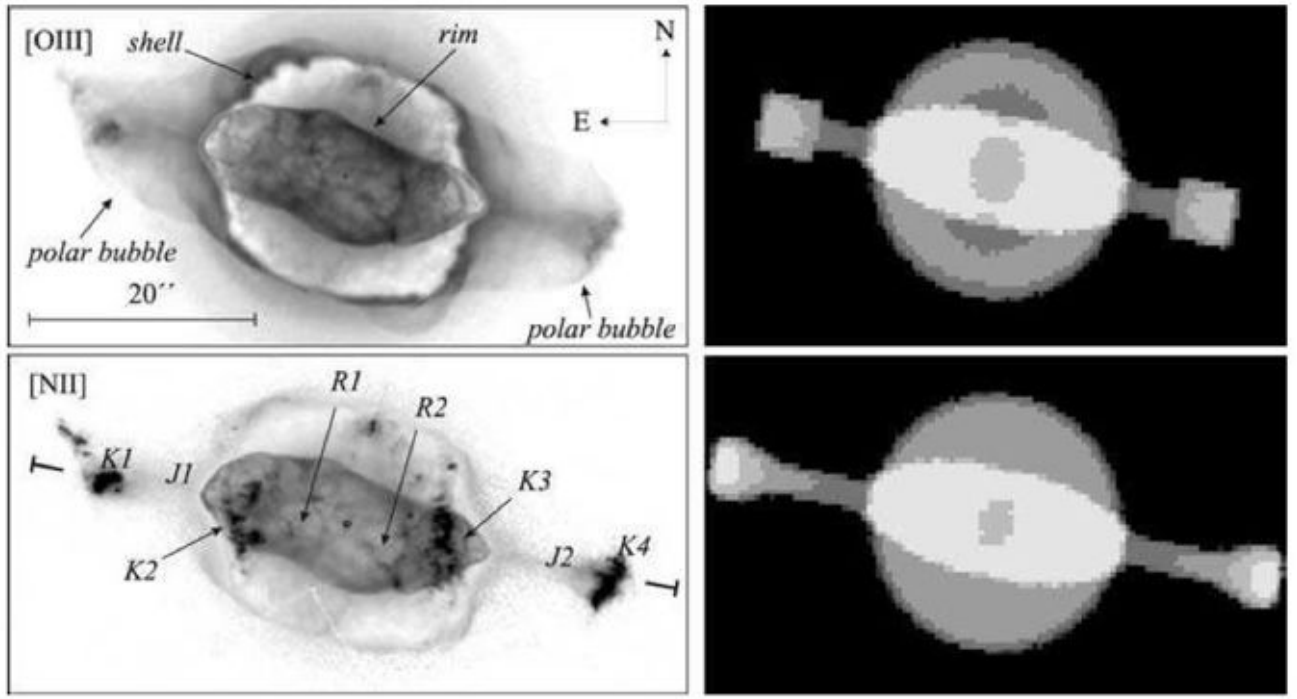

Figure 2. Left-hand panel: *HST* [O III] and [N II] images of NGC 7009 on a logarithmic intensity scale; slit position for the spectra discussed in Section 2.1 is indicated by short lines (PA = 79°), while labels mark the position of the several structures, where 'K', 'J' and 'R' stand for 'knot', 'jet' and 'rim', respectively. Right-hand panel: project emission maps from the model; the top map is [O III] and the bottom one is [N II]; maps (in arbitrary units) are not on the same colour-intensity scale.

On the nitrogen abundance of fast, low-ionization emission regions: the outer knots of the planetary nebula NGC 7009

D. R. Gonçalves,[1,3★] B. Ercolano,[2] A. Carnero,[2] A. Mampaso[3] and R. L. M. Corradi[3,4]

and [N II] images, and long-slit spectra of NGC 7009. Our model is indeed able to reproduce the main spectroscopic and imaging characteristics of the bright inner rim of NGC 7009 and its outer pairs of knots, assuming *homogeneous elemental abundances* throughout the nebula, for *nitrogen* as well as all the other elements included in the model.

Because of the fact that the $(N^+/N)/(O^+/O)$ ratio predicted by our models is 0.60 for the rim and is 0.72 for the knots, so clearly in disagreement with the $N^+/N = O^+/O$ assumption of the ionization correction factor (icf) method, the icfs will be underestimated by the empirical scheme, in both components, rim and knots, but more so in the knots. This effect is partly responsible for the apparent inhomogeneous N abundance empirically derived. The differences

Multiple stars

The effects of spatially distributed ionisation sources on the temperature structure of H II regions

B. Ercolano[1,2], N. Bastian[2], G. Stasińska[3]
[1] Harvard-Smithsonian Centre for Astrophysics, 60 Garden Street, Cambridge, MA 02138, USA
[2] Department of Physics and Astronomy, University College London, Gower Street, London WC1E 6BT, UK
[3] LUTH, Observatoire de Paris, CNRS, Université Paris Diderot ; Place Jules Janssen 92190 Meudon, France

Table 4. Oxygen abundances derived applying various metallicity indicators to the integrated emission line spectra calculated for our models (See text for calibrations used). All abundances are given in logarithmic scale, 12 + log(O/H). The input values of 12 + log(O/H) (i.e. 'the right answer') are 8.99 ($Z/Z_\odot = 2$), 8.69 ($Z/Z_\odot = 1$), 8.29 ($Z/Z_\odot = 0.4$), 7.99 ($Z/Z_\odot = 0.2$) and 7.39 ($Z/Z_\odot = 0.05$). $|\Delta|$, the largest difference between the abundance derived from C, H and F cases are given for each model trio. The value averaged over all models, $|<\Delta>|$, is given in the last row of the table.

model	O_{23}	O_3N_2	N_2	S_{23}	S_3O_3	Ar_3O_3	model	R_{23}	O_3N_2	N_2	S_{23}	S_3O_3	Ar_3O_3
CSp2.0	8.67	8.78	8.44	7.92	8.77	8.83	CSh2.0	8.62	8.77	8.50	8.09	8.75	8.82
HSp2.0	8.69	8.78	8.43	7.87	8.76	8.81	HSh2.0	8.62	8.77	8.50	8.08	8.75	8.82
FSp2.0	8.67	8.73	8.52	8.17	8.67	8.78	FSh2.0	8.63	8.76	8.52	8.16	8.72	8.81
$\|\Delta\|$	0.02	0.05	0.09	0.30	0.10	0.05	$\|\Delta\|$	0.01	0.01	0.02	0.08	0.03	0.01
CSp1.0	8.74	8.27	8.17	7.76	8.04	8.48	CSh1.0	8.66	8.30	8.24	7.94	8.16	8.55
HSp1.0	8.75	8.27	8.16	7.73	8.02	8.46	HSh1.0	8.67	8.30	8.23	7.92	8.14	8.54
FSp1.0	8.49	8.40	8.43	8.34	8.24	8.62	FSh1.0	8.51	8.38	8.39	8.23	8.24	8.61
$\|\Delta\|$	0.26	0.13	0.27	0.61	0.22	0.16	$\|\Delta\|$	0.16	0.08	0.16	0.31	0.10	0.07
CSp0.4	8.52	8.07	7.87	7.93	8.28	7.96	CSh0.4	8.52	8.09	7.97	8.49	8.10	7.77
HSp0.4	8.52	8.06	7.85	7.92	8.22	7.91	HSh0.4	8.50	8.10	7.98	8.45	8.08	7.73
FSp0.4	8.43	8.24	8.15	8.22	9.02	8.25	FSh0.4	8.41	8.23	8.19	8.92	8.27	8.12
$\|\Delta\|$	0.09	0.18	0.30	0.30	0.80	0.34	$\|\Delta\|$	0.11	0.14	0.22	0.47	0.19	0.39
CSp0.2	7.86	7.97	7.77	7.99	7.67	7.67	CSh0.2	7.84	7.99	7.79	8.18	7.87	7.92
HSp0.2	7.87	7.97	7.77	8.01	7.66	7.66	HSh0.2	7.86	7.97	7.77	8.10	7.79	7.82
FSp0.2	7.68	8.15	8.05	8.68	8.10	8.26	FSh0.2	7.72	8.13	8.02	8.61	8.11	8.26
$\|\Delta\|$	0.19	0.18	0.28	0.69	0.44	0.60	$\|\Delta\|$	0.14	0.16	0.25	0.51	0.32	0.44
CSp0.05	7.48	7.92	7.51	7.29	7.39	6.30	CSh0.05	7.44	7.93	7.51	7.38	7.58	6.67
HSp0.05	7.44	7.95	7.56	7.37	7.49	6.51	HSh0.05	7.44	7.94	7.53	7.38	7.57	6.63
FSp0.05	7.15	8.12	7.77	7.73	7.91	7.48	FSh0.05	7.21	8.09	7.74	7.69	7.93	7.49
$\|\Delta\|$	0.33	0.20	0.26	0.44	0.52	1.18	$\|\Delta\|$	0.23	0.16	0.23	0.31	0.36	0.86
$<\|\Delta\|>$	0.18	0.15	0.24	0.47	0.41	0.47	$<\|\Delta\|>$	0.12	0.11	0.18	0.32	0.23	0.45

The abundance determinations show strong biases due to the presence of multiple HII regions summed in the same observation.

Complete example

The chemical composition of TS 01, the most oxygen-deficient planetary nebula

AGB nucleosynthesis in a metal-poor binary star⋆,⋆⋆,⋆⋆⋆

G. Stasińska[1], C. Morisset[2], G. Tovmassian[3], T. Rauch[4], M. G. Richer[3], M. Peña[2], R. Szczerba[5], T. Decressin[6], C. Charbonnel[7], L. Yungelson[8], R. Napiwotzki[9], S. Simón-Díaz[10], and L. Jamet[1]

- No Te-diagnostics ([Nev]λ24.3μm/[Ne v] λ3426, but need good cross-calibration, with aperture effects)
- Complexe SED (2 stars, both acting on the nebula)
- Complexe morphology (Bipolar shape)

BUT :

- Good stellar observations to constraint the central engine
- Good and multiple observations of the nebula (IR-opt-UV spectra + images).
- C3D photoionization code to take into account morphology and slit positions

Complete example

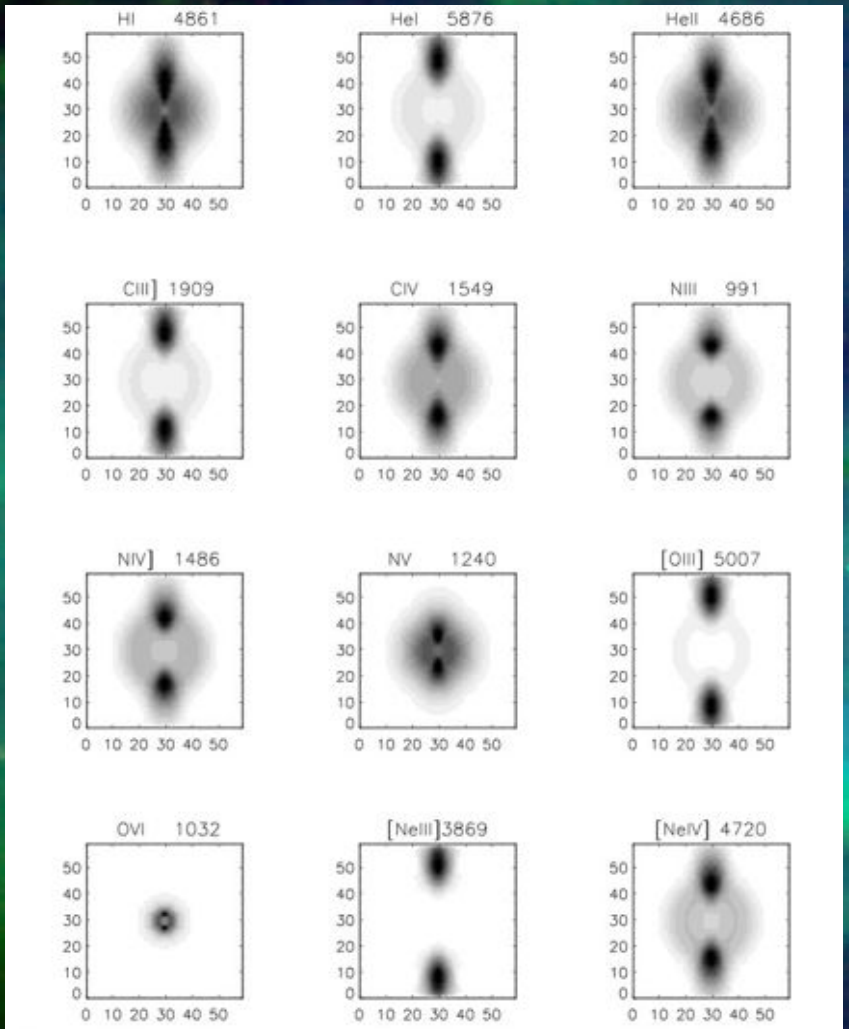

Fig. 14. Monochromatic images of the reference model in various lines (the values of the wavelengths are in Å if they are larger than 900, and in μm otherwise). The x and y values are the coordinates in pixel units of the models.

Table 6. Nebular abundances of TS 01, in various units.

	12+log X/H	Uncertainty	X/H	Mass fraction
He	10.95	±0.04	8.91×10^{-2}	2.63×10^{-1}
C	7.84	±0.30	6.92×10^{-5}	6.11×10^{-4}
N	7.15	±0.25	1.41×10^{-5}	1.46×10^{-4}
O	6.82	±0.33	6.61×10^{-6}	7.79×10^{-5}
Ne	6.83	±0.30	6.76×10^{-6}	9.96×10^{-5}
S	<5.5		$<3.16 \times 10^{-7}$	$<7.45 \times 10^{-6}$
Ar	<4.5		$<3.16 \times 10^{-8}$	$<8.38 \times 10^{-7}$

Oxygen and other elemental abundances are determined within 0.3 dex error, quite good without Te-diagnostic!

On N-component models

- Adding N photoionization models weighted by covering factors can represent very different topological distributions of the N components.
- Cloudy_3D is one of the use of this, where a spatial distribution is assumed.
- t^2 can be simulated by adding extra heating in some part of the nebula, even without knowing exactly why it occurs and where it is located.

On N-component models

RESOLVING THE ELECTRON TEMPERATURE DISCREPANCIES IN H II REGIONS AND PLANETARY NEBULAE: κ–DISTRIBUTED ELECTRONS

DAVID C. NICHOLLS[1], MICHAEL A. DOPITA[12], & RALPH S. SUTHERLAND[1]

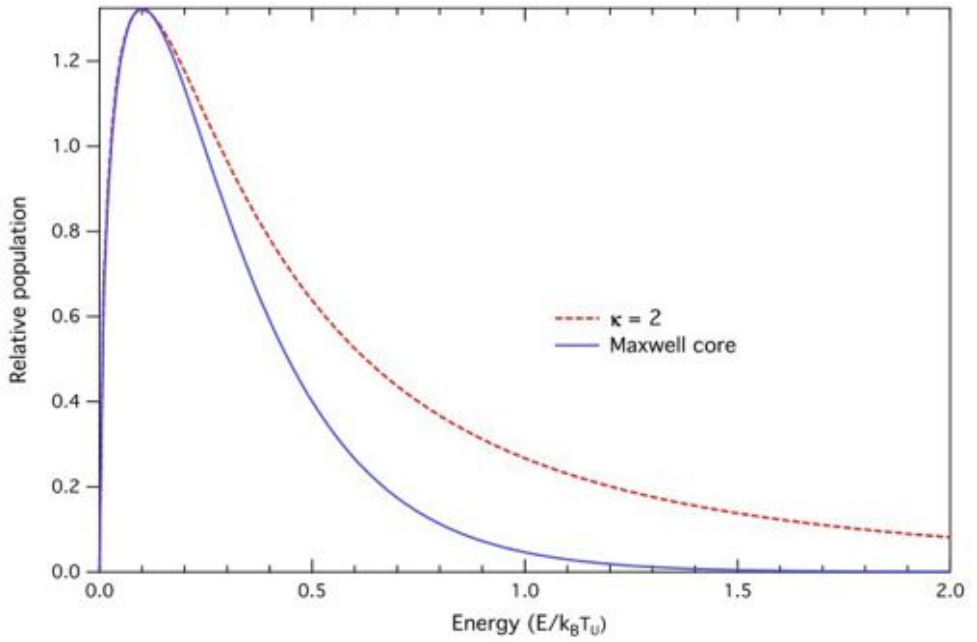

FIG. 4.— $\kappa = 2$ energy distribution with peak-fitted Maxwell-Boltzmann distribution core.

- The spatial distribution of the N components can even be microscopic instead of macroscopic → Kappa distribution as a sum of gaussians
- Each gaussian corresponds to a fraction of the gas being at a different temperature, obtained by adding extra heating to different runs of photoionization models.

Conclusions

- Photoionization modeling is sometimes more efficent than direct method as it can take into account coherently and simultaneously all the observables of a given object, as well as aperture, dust, N-components, and 3D effects.
- But it takes more time and experience to be correctly converged, and
- It also needs that the electron temperature is well constraint (or by diagnostic, or by controlling almost everything).